Thermal Decomposition of Furan Generates Propargyl Radicals

AnGayle Vasiliou,[†] Mark R. Nimlos,*[,‡] John W. Daily,*[,§] and G. Barney Ellison*[,†]

Department of Chemistry and Biochemistry, University of Colorado, Boulder, Colorado 80309-0215, National Renewable Energy Laboratory, 1617 Cole Boulevard, Golden, Colorado 80401, and Center for Combustion and Environmental Research, Department of Mechanical Engineering, University of Colorado at Boulder, Boulder, Colorado 80309-0427

Received: April 13, 2009; Revised Manuscript Received: June 10, 2009

The thermal decomposition of furan has been studied by a 1 mm × 2 cm tubular silicon carbide reactor, $C_4H_4O + \Delta \rightarrow$ products. Unlike previous studies, these experiments are able to identify the initial furan decomposition products. Furan is entrained in either He or Ar carrier gas and is passed through a heated (1600 K) SiC tubular reactor. Furan decomposes during transit through the tubular reactor (approximately 65 μs) and exits to a vacuum chamber. Within one nozzle diameter of leaving the nozzle, the gases cool to less than 50 K, and all reactions cease. The resultant molecular beam is interrogated by photoionization mass spectroscopy as well as infrared spectroscopy. Earlier G2(MP2) electronic structure calculations predicted that furan will thermally decompose to acetylene, ketene, carbon monoxide, and propyne at lower temperatures. At higher temperatures, these calculations forecast that propargyl radical could result. We observe all of these species (see Scheme 1). As the pressure in the tubular reactor is raised, the photoionization mass spectra show clear evidence for the formation of aromatic hydrocarbons.

I. Introduction to Biomass Gasification

Biomass gasification is a mature technology that has been empirically used for nearly a century. Thermochemical processing[1−3] is used to convert solid biomass into clean liquid fuels and chemicals. Biomass is plant material such as agricultural crops, trees, and grasses. Composed of the structural polymers cellulose, hemicellulose, and lignin, along with a variety of volatile compounds called extractives, biomass provides a significant source of hydrocarbons. Thermochemical processing involves heating of the feedstock under controlled conditions. The three main approaches are direct combustion for heat generation, gasification to generate syngas, and pyrolysis used to produce liquids. (Here, the term pyrolysis is used as the industrial meaning of the process that produces liquids. The normal definition is heating in the absence of oxygen, and that will be our use henceforth.)

One aspect that all thermal methods share is the use of heat to break the chemical bonds of the large structural biopolymers into smaller semivolatile or volatile units and char.[4,5] Heating first raises the feedstock to the boiling temperature of liquid water, which must be completely vaporized before further heating occurs. As the temperature rises above about 500 K, thermal decomposition begins to occur. The gaseous decomposition products are then driven to the surface and become available to react in the gas phase. The physical problem of heating, drying, and pyrolyzing is extremely complex. It involves conduction and convection in porous media, decomposition chemistry, and subsequent gas-phase chemistry. There are also possible catalyst effects as the gaseous products flow through already charred outer layers of the solid. Local heating rates can vary by several orders of magnitude.

Biomass heating results in a mix of gaseous volatile compounds and semivolatile compounds that liquefy into tars and solid char. It has long been the goal of those studying thermochemical processing to be able to predict both the primary decomposition products and their subsequent reaction chemistry. However, no experiments to date have been able to resolve the chemistry on a time scale and with speciation accuracy that would provide detailed kinetics information. As a result, workers who have studied the decomposition kinetics have been forced to settle for developing simple global mechanisms. An example that is commonly cited in the literature is the Diebold mechanism[6] for cellulose. This model and other similar mechanisms[5,7] constitute the current state of the art.

Diebold's Cellulose Decomposition Scheme

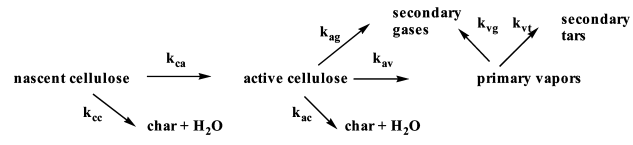

(1)

Cellulose (40−50% by mass of biomass) is a linear polymer[8] of cellobiose (the 1,4′ dimer of glucopyranose). The sugars form long chains that then cross-link via weaker hydrogen bonding.[9,10] The cross-links break readily upon heating. In the literature, the term "activated cellulose" has been used to describe the state where most of these bonds have broken. Upon further heating, the β-1,4′-glycosidic linkages between D-glucose begin to break, as do other bonds, producing a broad spectrum of compounds. The Diebold mechanism (or others like it) can be used to estimate overall decomposition rates. In Figure 1, the mass fraction versus time for the "species" identified by Diebold are shown. In this result, the initial stock is converted to active

* To whom correspondence should be addressed. E-mail: barney@jila.colorado.edu (G.B.E.); mark_nimlos@nrel.gov (M.R.N.); john.daily@colorado.edu (J.W.D.).
† Department of Chemistry and Biochemistry, University of Colorado.
‡ National Renewable Energy Laboratory.
§ Department of Mechanical Engineering, University of Colorado at Boulder.

10.1021/jp903401h CCC: $40.75
Published on Web 07/06/2009

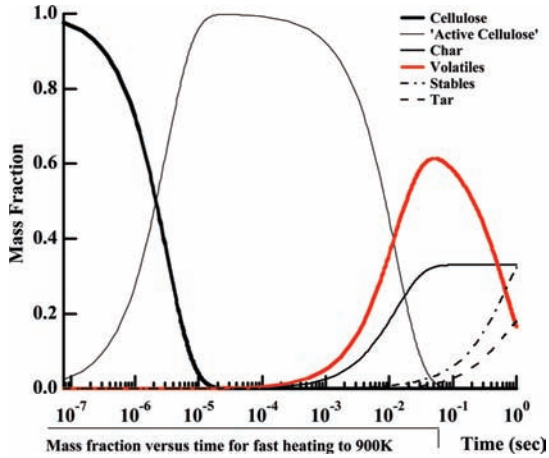

Figure 1. A simulation of the kinetics of eq 1.

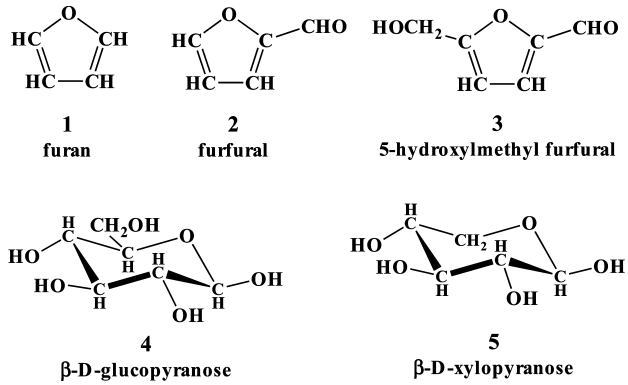

Figure 2. The structures of several biomass monomers.

cellulose in about 10 μs. The rate-limiting steps are then the conversions from the active form into stable gases, semivolatiles that subsequently condense to tars, and char.

Furanyl compounds are important intermediates in the thermochemical decomposition of biomass (the "volatiles" in Figure 1). For instance, furan, **1**, furfural, **2**, and 5-hydroxymethylfurfural, **3**, have been detected during the pyrolysis of plant material[11−14] (see Figure 2). These species are largely thought to evolve from the thermal decomposition of the polysaccharides that are the principal components of plant cell walls. Separate pyrolysis experiments with these polysaccharides,[15−17] cellulose and hemicellulose, appear to bear this out. The structures of glucose, **4**, and xylose, **5**, are also shown.

Although these molecules have been measured during biomass pyrolysis, which is typically conducted at 700−900 K, their contribution to high-temperature conversion processes is not clear. Consider biomass gasification, which can be followed by catalytic synthesis to produce a variety of transportation fuels. During gasification for fuel synthesis, the biomass is typically heated to between 1000 and 1250 K using H_2O (steam) as a carrier gas.[18]

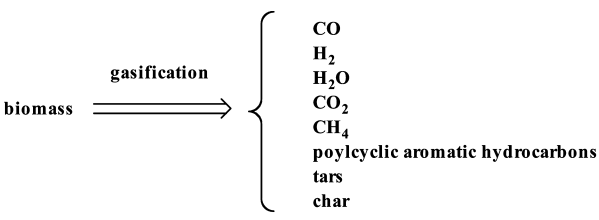

(2)

Clean syngas (CO and H_2) is the desired product from this process, though in reality, CO_2, CH_4, polycyclic aromatic (PAH) hydrocarbons, tars, and char are also produced (eq 2). As an example of

SCHEME 1

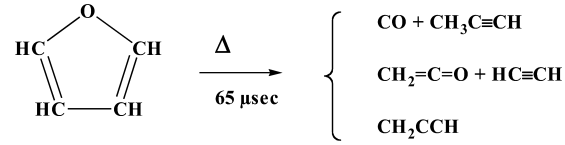

fuel synthesis, the CO and H_2 can be catalytically combined to produce ethanol, as depicted in eq 3.

$$2CO + 4H_2 \xrightarrow{\text{catalyst}} CH_3CH_2OH + H_2O \qquad (3)$$

This approach for renewable fuel synthesis is nearly economically competitive for a variety of fuel feedstocks.[18]

In order to minimize tar formation during biomass gasification, a better understanding of formation reaction mechanisms is needed. Specifically, it is desirable to understand the mechanism for the formation of PAHs. Since the polysaccharides comprise up to 70% of plant cell walls, it is necessary to understand how their decomposition leads to the formation of PAHs.

It is likely that furans play an important role in PAH formation from sugars since these aromatic species appear to result from dehydration reactions of carbohydrates. Experimental measurements (vide infra) of the thermal decomposition of furan show that small hydrocarbon molecules,[19−24] such as acetylene, ketene, and propyne, are formed. In addition, some shock tube studies show that benzene can be produced.[24] This earlier work on the thermal decomposition of furan used techniques that were not effective for detecting radicals, which will likely play an important role in the formation of aromatic compounds.

We surmise that there is a link between carbohydrates and the formation of aromatic hydrocarbons. When heated, (1) carbohydrates dehydrate to a mixture of furanyl compounds, (2) furanyl species further decompose into smaller molecular fragments, which (3) ultimately recombine in less than 1 msec to form aromatic molecules. In this paper, the connection between the simplest furanyl species, furan (**1** in Figure 2) and aromatic compounds will be investigated. Results will be presented for pyrolysis of furan, **1**, in a heated, supersonic nozzle,[25−28] C_4H_4O (furan) + $\Delta \rightarrow$ products. The resulting products are measured using vacuum-ultraviolet photoionization mass spectrometry (PIMS) and matrix isolation infrared spectroscopy (IR). The combination of these approaches has been successfully used in the past[26,29−31] to detect radicals and measure their infrared spectra. In this paper it will be shown that, along with the closed-shell molecules measured earlier, furan decomposes to produce propargyl (CH_2CCH) radicals. We have also observed the formation of benzene and other aromatic species from the thermal cracking products of furan.

II. Experimental Methods

A high-temperature miniature flow reactor (hyperthermal nozzle)[28] (Figures 3 and 4) can be used to decompose simple biomass molecules such as furan (**1** in Figure 2). Thermal cracking products are produced by pulsing C_4H_4O (furan) seeded in an inert gas (roughly 1−2 atm) through a resistively heated silicon carbide tube (1 mm ID, about 2 cm long) at high temperature (up to 1700 K) into a vacuum chamber (about 10^{-5} Torr). The valve fires at a nominal rate of 10−50 Hz and is open for roughly 250 μs. The gas is injected into the tube through a small orifice, where the flow is choked, controlling the mass flow rate. The residence time in the heated section of

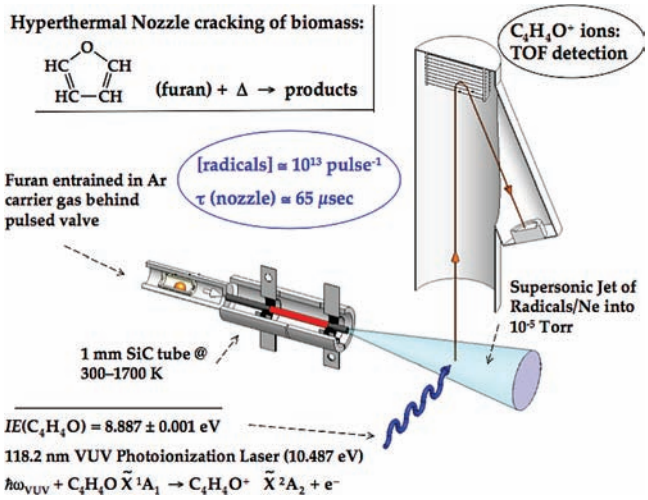

Figure 3. Schematic view of the hyperthermal nozzle for thermal cracking of biomass samples with PIMS detection.

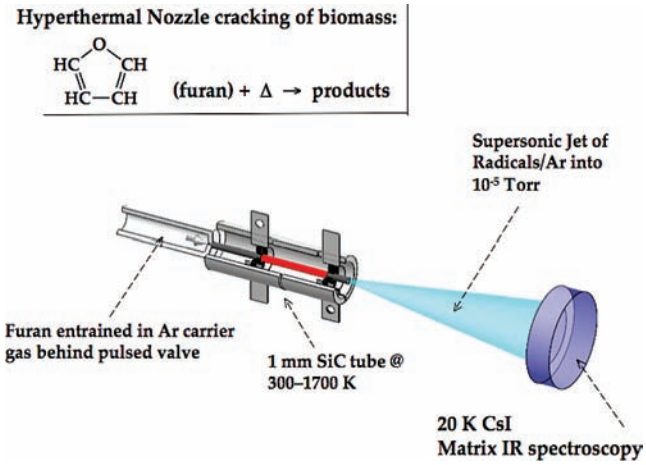

Figure 4. Schematic view of the hyperthermal nozzle for thermal cracking of biomass samples with IR detection.

the tube is roughly 65 μs, which, combined with low sample density, avoids radical−radical reactions following thermal decomposition. The tube flow chokes at the exit and expands supersonically in an underexpanded jet to a vacuum at 10^{-5} Torr. This free jet expansion rapidly cools the radicals down to about 40 K (rotationally)[32] within approximately a tube diameter and eliminates any further reactions. We have used two independent spectroscopic techniques to monitor the output of the hyperthermal nozzle. The nozzle in Figure 3 uses a fixed frequency ($\lambda_0 = 118.2$ nm) photoionization mass spectrometer to detect the species emerging from the nozzle. Figure 4 shows the high-temperature nozzle configured in a different way, in which the beam impinges onto a 20 K CsI window, forming a matrix for IR detection. The combination of high nozzle wall temperature (up to 1700 K) and short residence time allows for high yield of radicals (approximately 10^{13} radicals pulse^{-1}).

The photoionization TOF mass spectrometer that was used in these experiments has been described in more detail elsewhere,[33] and we will only provide a brief description here. The output of our hyperthermal nozzle is pulsed into a vacuum chamber (10^{-5} Torr) and then directed through a skimmer (3 mm ID) into a ionization vacuum chamber (10^{-7} Torr), where radicals are ionized using vacuum-ultraviolet photons (118.2 nm or 10.487 eV with 0.5 μJ/pulse at 10−30 Hz). The mass spectra are collected using a reflectron TOF mass spectrometer (Jordan). The positive ions are detected by a channeltron, and the spectra are collected with a digital oscilloscope (Tektronix 500 MHz) interfaced to a computer. Typically, averaging of 100−1000 pulses is needed to obtain mass spectra with reasonable signal-to-noise, and because the laser is pulsed at 10 Hz, scans are collected in 1−2 min. As a result, mass spectra at several temperatures can be obtained in 20−30 min. These experiments are much faster than the matrix isolation experiments, which require about 4−6 h for an experiment at a single temperature.

The photoionization mass spectrometer was calibrated prior to all experiments discussed in this work. Using NO, $CH_3CH{=}CH_2$, or $C_6H_5CH_3$ as the calibrant with well-characterized cracking patterns, flights times ranging from 10 to 100 μs were used to construct a calibration curve. The calibration process was repeated during and at the end of each experiment to ensure that significant drift did not occur in the TOF electronics or PIMS instrument. All peaks in the resulting mass spectra were accurate to within ±0.2 amu.

In Figure 4, the hyperthermal nozzle was mounted to the vacuum shroud of an APD two-stage closed-cycle helium cryostat, approximately 2.5 cm away from the cryogenic CsI window. Gas mixtures were created by seeding a precursor in argon. The precursor vapor was collected by degassing the precursor liquid at room temperature. The hyperthermal nozzle was operated with approximately a 1.3 ms pulse width and a stagnation pressure of 1.2 atm, with a 1.2 L stagnation reservoir. The pressure drop in the stagnation reservoir was measured using a capacitance monometer to determine the gas throughput. Radicals were deposited on a CsI salt window cryogenically cooled to 20 K. The infrared spectrum of the sample was measured using a Nicolet Magna 550 Fourier transform infrared spectrometer with a mercury/cadmium/telluride (MCT-A or B) detector. The APD cryostat was equipped with a pair of CsI side windows, through which the IR beam from the instrument passes.

III. Results: Thermal Decomposition of Furan

The high-temperature supersonic nozzle in Figure 3 is an appealing device to study the thermal decomposition of isolated biomass targets in rare gases. Because the nominal residence time of the entrained furan in the hot nozzle is roughly 65 μs, we are able to monitor the early fragmentation products. Classical gravimetric analysis of biomass decomposition leads to the kinetic picture sketched in Figure 1. The nascent cellulose has completely decomposed in 10 μs, and the reactive volatiles (shown in red) begin to appear in approximately 1 msec. The hot nozzle in Figures 3 and 4 with PIMS and matrix IR detection permits us to examine the early thermal cracking products.

The thermal decomposition of furan has been studied in flow tubes,[19,23] shock tubes,[21,22,24] and by IR homogeneous pyrolysis.[20] A summary of these results is collected in Table 1. These studies have been conducted over a wide range of pressures (1 mTorr−20 atm) and temperatures (500−3000 K), and it is commonly agreed that there are two major decomposition channels.

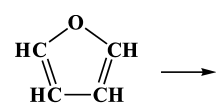

a) $CO + CH_3C{\equiv}CH$

b) $CH_2{=}C{=}O + HC{\equiv}CH$ (4)

The thermochemistry of these two pathways is well-known.[34,35]

TABLE 1: Previous Measurements of the Thermal Decomposition of Furan

apparatus	conditions	notes	ref
very low pressure pyrolysis (VLPP)	1050−1270 K at 1 mTorr; EI mass spectrometry	$CO + C_3H_4$	19
shock tube	1050−1460 K; GC/FID	major channels: $CO + CH_3CCH$, $HCCH + CH_2CO$ $CH_2{=}C{=}CH_2$, C_4H_6, C_2H_4, CH_4, C_4H_4, C_4H_2, and C_6H_6	24
flow tube	960−1085 K at 1 Torr	$CO + C_3H_4$	23
shock tube	1100−1700 K at 20 atm; UV, FTIR	$CO + C_3H_4$, $HCCH + CH_2CO$	22
shock tube	500−3000 K at 600 Torr; laser-schlieren densitometry; TOF-MS	major channels: $HC{\equiv}CH + CH_2CO$, $C_3H_4 + CO$; below 1700 K, $C_3H_4 + CO$ channel dominates	21
IR homogeneous pyrolysis	GC-MS/FID, FTIR, EPR; CO_2 10.6 μm irradiation of 7 Torr of SF_6 followed by heating via rapid inter- and intramolecular relaxation. Hot SF_6 heats furan.	major channels: $HC{\equiv}CH + CH_2CO$, $C_3H_4 + CO$	20

$$\Delta_{rxn}H_{298}(C_4H_4O, \text{furan} \rightarrow CO + CH_3C{\equiv}CH) = 26.1 \pm 0.3 \text{ kcal mol}^{-1} \quad (5a)$$

$$\Delta_{rxn}H_{298}(C_4H_4O, \text{furan} \rightarrow CH_2{=}C{=}O + HC{\equiv}CH) = 51.3 \pm 0.5 \text{ kcal mol}^{-1} \quad (5b)$$

In Figure 5 are shown the PIMS spectra of the decomposition products of furan in a high-temperature supersonic nozzle. At lower nozzle temperatures, we observe decomposition products which are consistent with the shock tube temperatures reported by Fulle et al.[21] (900−1500 K) and others in Table 1. The bottom trace in Figure 5 is the mass spectrum that results when furan (1 Torr of C_4H_4O entrained in 2 atm of He) transits the nozzle at room temperature (300 K). Photoionization with 118.2 nm VUV light produces the parent ion, m/z 68 $C_4H_4O^+$, and its isotope peak, m/z 69. The (69/68) isotope ratio is measured to be 5%. The *IE*(furan) was measured[36] to be 8.887 ± 0.001 eV; even though C_4H_4O is ionized by 10.487 eV photons, no fragmentation of the parent ion $C_4H_4O^+$ is observed. When the wall temperature of the SiC nozzle is raised to 1500 ± 100 K,

Figure 5. PIMS spectra of the decomposition products of furan in a high-temperature supersonic nozzle. The bottom trace is the mass spectrum that results when furan (1 Torr of C_4H_4O entrained in 2 atm of He) transits the nozzle at room temperature (300 K).

Figure 6. PIMS spectra for appearance of decomposition products from furan as the wall temperature of the nozzle is increased.

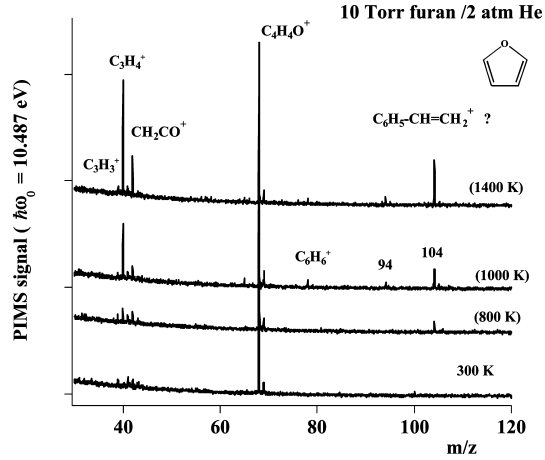

Figure 7. PIMS spectra of the decomposition products of higher concentrations of furan (10 Torr of C_4H_4O entrained in 2 atm of He) in a high-temperature supersonic nozzle.

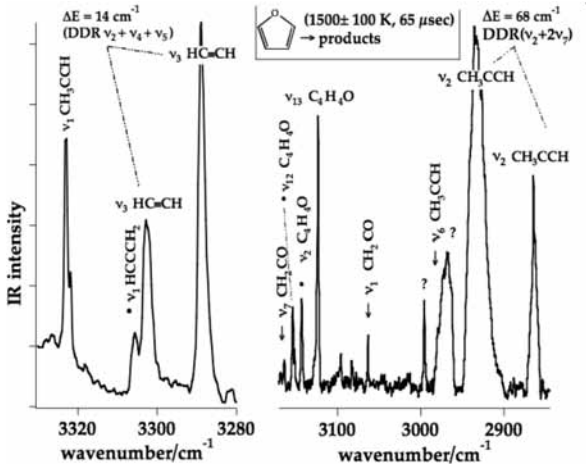

Figure 8. Infrared spectrum of the decomposition products of furan at 1500 ± 100 K. The presence of the propargyl radical is revealed by the intense $\nu_1(CH_2CC-H)$ stretch[26] at 3309 cm^{-1}.

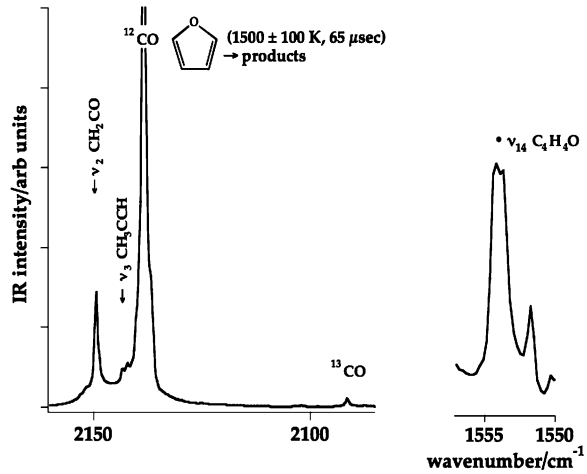

Figure 9. Infrared spectrum of the decomposition products of furan at 1500 ± 100 K. Both ketene and carbon monoxide (^{12}CO and ^{13}CO) are clearly present.

product ions at *m/z* 40 and 42 are observed, which arise from ionization[37−39] of C_3H_4 and CH_2CO. Increasing the wall temperature to 1650 ± 100 K leads to an increase in the $C_3H_4^+$ and CH_2CO^+ signals, and new features at *m/z* 39 and 41 are detected. The band at *m/z* 41 is consistent with the ketene isotope peak. The (41/40) isotope ratio is calculated to be 3% for $C_3H_4^+$.

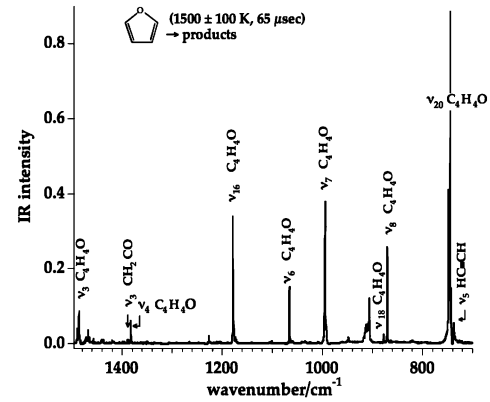

Figure 10. Infrared spectrum of the decomposition products of furan at 1500 ± 100 K. Distinctive bands of CH_2=C=O and HC≡CH can be identified.

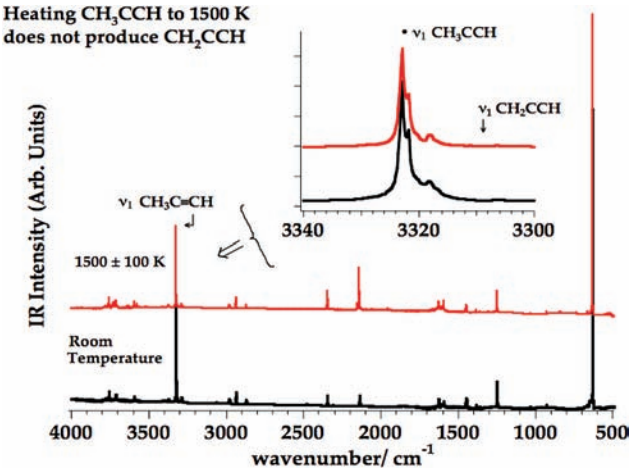

Figure 11. The bottom trace in this figure compares the matrix IR spectrum of CH_3C≡CH heated to 1500 K with a sample of methylacetylene that was deposited at room temperature. The spectra appear identical.

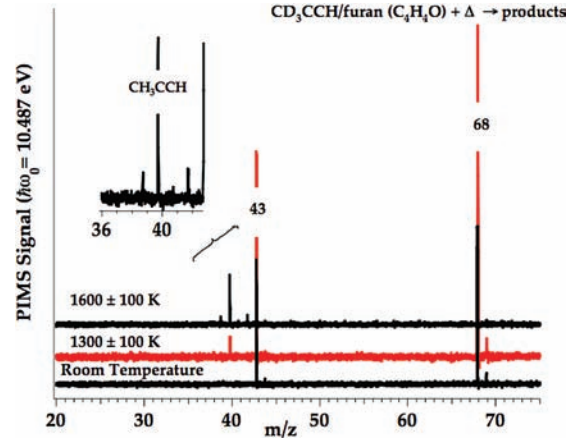

Figure 12. PIMS spectra of a 1:1 mixture of CD_3CCH and C_4H_4O passed through the SiC nozzle at temperatures of 300, 1300 ± 100, and 1600 ± 100 K.

We believe that the signal at *m/z* 39 is CH_2CCH^+ and is a diagnostic for the presence of the propargyl radical. The *IE*(CH_2CCH) has been measured by fixed frequency photoelectron spectroscopy and by ZEKE spectroscopy[40] to be 69953 ± 10 cm^{-1} (8.674 ± 0.001 eV). [Because[41] the *IE*(HCC) = 11.645 ± 0.0014 eV, it is unlikely that the VUV laser could ionize the CH_3CC radical.] As with the case of furan, photoionization of CH_2CCH by 118.2 nm photons does not induce fragmentation

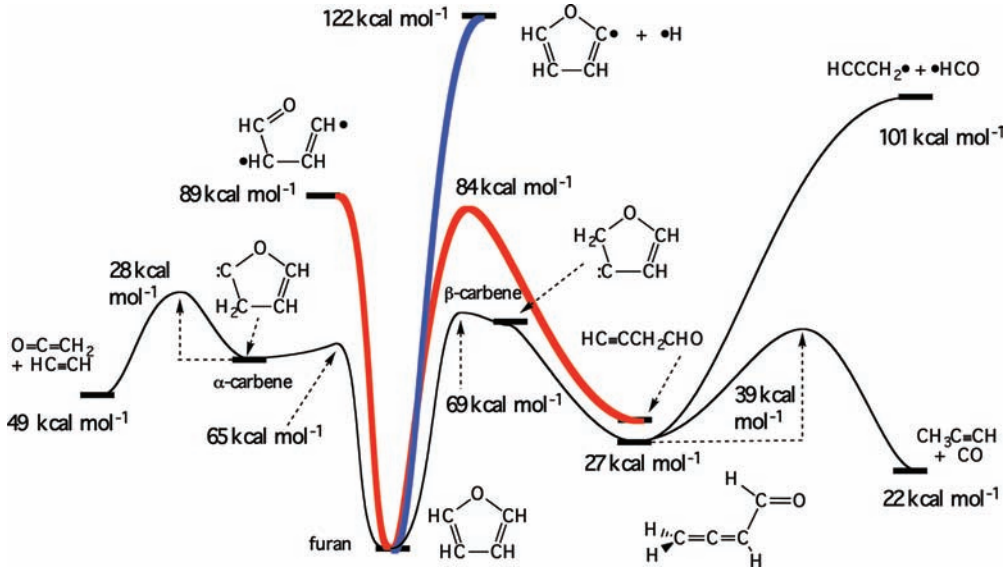

Figure 13. Potential energy surface for the decomposition of furan at 0 K. These are G2(MP2) calculations, and this figure is a composite adapted from Sendt et al.[58]

(even though the VUV laser is 1.8 eV above the threshold to ionize the propargyl radical). Notice that some of the thermal cracking products of furan in eq 5a cannot be photoionized by the 10.487 eV VUV laser in Figure 3, H atom $IE(H) = 13.5984 \pm 0.0001$ eV, acetylene[41] $IE(HC{\equiv}CH) = 11.4006 \pm 0.0006$ eV, and carbon monoxide[42] $IE(CO) = 14.0141 \pm 0.0003$ eV.

Figure 6 shows the PIMS spectra for the appearance of decomposition products from furan as the temperature of the nozzle is increased. At a wall temperature of 1350 ± 100 K, features for both $C_3H_4^+$ *m/z* 40 and CH_2CO^+ *m/z* 42 appear. At 1500 ± 100 K, faint signals for *m/z* 39 and 41 are observed. The *m/z* 41 feature is 5% as intense as the $C_3H_4^+$ *m/z* 40 signal and is likely the isotope peak. As the wall temperature of the nozzle is steadily increased to 1650 ± 100 K, the *m/z* 39 peak (propargyl radical) steadily grows.

If the concentration of furan is raised (10 Torr of C_4H_4O entrained in 2 atm of He), bimolecular reactions are observed; see Figure 7. In addition to the parent $C_4H_4O^+$ feature at *m/z* 68, all of the peaks present in Figures 5 and 6 are present (39, 40, 41, and 42). New features at *m/z* 78 ($C_6H_6^+$), 94 ($C_6H_5OH^+$), and 104 ($C_6H_5CH{=}CH_2^+$) are now present.[43−45] The spectra in Figure 7 were produced by a contaminated nozzle (see background signals around *m/z* 39−43 in the 300 K trace). However, it is clear that the features at *m/z* 78, 94, and 104 are growing in as the nozzle gets hotter. These species [probably benzene (78), phenol (94), and styrene (104)] certainly arise from bimolecular reactions among decomposition products of furan.

The PIMS spectra in Figures 5−7 are very informative, but they only identify molecular products by *m/z*, the mass-to-charge ratio. Isomers are always a problem, and some important molecules (CO and HCCH) cannot be detected by the 118.2 nm VUV laser. In Figure 8 are shown the infrared spectra of the decomposition products of furan at 1500 ± 100 K. This scan reveals CH peaks for CH_3CCH, HCCH, furan (C_4H_4O), and $CH_2{=}C{=}O$. The presence of the propargyl radical is revealed by the intense $\nu_1(CH_2CC{-}H)$ stretch[26] at 3309 cm^{-1}.

In Figure 9 is the infrared spectrum of the decomposition products of furan at 1500 ± 100 K in the mid-IR region. Carbon monoxide (both isotopomers ^{12}CO and ^{13}CO) and $CH_2{=}C{=}O$ are clearly present. Figure 10 is the infrared spectrum of the decomposition products of furan at 1500 ± 100 K over the fingerprint region. Distinctive bands of $CH_2{=}C{=}O$ and $HC{\equiv}CH$ can be identified as decomposition products.

One of the shock tube studies[24] reports $CH_2{=}C{=}CH_2$ as a cracking product of furan. It is possible that the PIMS signal at *m/z* 40 could be evidence of allene rather than CH_3CCH. The IR spectrum of allene is well-known, but the IR spectra in Figures 8−10 show no bands of $CH_2{=}C{=}CH_2$. Both the PIMS traces and IR spectra provide convincing evidence of both CH_3CCH (propyne) and CH_2CCH (propargyl radical). One might suspect that propyne is thermally cracked at higher temperatures to produce propargyl, $CH_3CCH + \Delta \rightarrow CH_2CCH + H$. The bond energies of methylacetylene have been measured,[46] and $\Delta H_{298}(H{-}CH_2CCH)$ is known to be 90 kcal mol^{-1}. Consequently, it is very unlikely that the hyperthermal nozzle could induce propyne to dissociate to $CH_2CCH + H$. The bottom trace in Figure 11 compares the matrix IR spectrum of $CH_3C{\equiv}CH$ heated to 1500 K with a sample of methylacetylene that was deposited at room temperature. The spectra are identical. The strong C−H stretching mode for CH_3CCH is identified at 3322.8 cm^{-1}. The inset at the top of the spectrum is an expanded scan of the region about $\nu_1(CH_3CC{-}H)$. There is no detectable signal for the intense $\nu_1(CH_2CC{-}H)$ stretch[26] of the propargyl radical at 3309 cm^{-1}. A similar attempt to observe thermal cracking at 1500 ± 100 K of d_3-methylacetylene, $CD_3CCH + \Delta \rightarrow CD_2CCH + D$, with the PIMS in Figure 3 also failed. When d_3-metylacetylene is passed through the nozzle at 300 or 1500 K, the PIMS only detects the parent species, $(CD_3CCH)^+$ *m/z* 43, and no signals from d_2-propargyl, $(CD_2CCH)^+$ *m/z* 41, are observed.

To further confirm that propargyl radical is a direct product of furan decomposition, a 1:1 mixture of CD_3CCH and C_4H_4O was passed through the SiC nozzle at temperatures of 300, 1300 ± 100, and 1600 ± 100 K. The resulting PIMS spectra are shown in Figure 12; intense features at *m/z* 43 $(CD_3CCH)^+$ and 68 $(C_4H_4O)^+$ are evident at room temperature. One expects the isotope for CD_3CCH and furan to be 3.2 and 4.4%. The measured ratios are (44/43) = 3% and (69/68) = 5%.

As the nozzle temperature is raised to 1300 K, fragmentation of the CD_3CCH/furan mixture commences. At 1600 ± 100 K, the inset shows new bands at *m/z* 39 $(CH_2CCH)^+$, 40 $(CH_3CCH)^+$, 41, and 42 $(CH_2{=}C{=}O)^+$ are observed. The feature at *m/z* 41 could be CD_2CCH^+ or the isotope peak related

to the CH_3CCH cracking product of furan. The (41/40) ratio in the 1600 K scan in Figure 12 is measured to be 4%. The CH_3CCH (41/40) isotope ratio is expected to be 3.2%. We conclude that the peak at *m*/*z* 41 is the isotope peak belonging to the CH_3CCH, which results from cracking of furan.

The IR spectra in Figure 11 and the PIMS spectra of Figure 12 are consistent. Heating $CH_3C{\equiv}CH$ to 1500 K does not produce the propargyl radical, CH_2CCH. Consequently CH_2CCH, *m*/*z* 39, in Figure 5 is a direct decomposition product of furan itself.

IV. Discussion and Conclusions

These experiments have enabled us to identify the initial thermal cracking products of furan. Using a high-temperature nozzle as a tubular reactor, we have demonstrated that furan thermally cracks to produce (CO + CH_3CCH) and (HCCH + CH_2CO). This is expected from eq 4 and the earlier studies in Table 1. When the wall temperature reaches 1350 ± 100 K, all of these species are detected by both the PIMS and IR spectrometers of Figures 3 and 4. At a higher temperature of 1550 ± 100 K, furan (C_4H_4O) begins to produce the propargyl radical (CH_2CCH) as well. Because the residence time of the furan in the tubular reactor is roughly 65 μs, we believe that (CO + CH_3CCH), (HCCH + CH_2CO), and the CH_2CCH radical are the primary products from cracking of C_4H_4O. Increasing the backing pressure of the carrier gas by an order of magnitude leads to the formation of aromatic hydrocarbons such as benzene and styrene (Figure 7). It is well established[47−57] that propargyl radicals dimerize to produce C_6H_6. In an earlier study with this apparatus,[26] CH_2CCH radicals were observed to form C_6H_6; both PIMS and IR spectroscopy were used to confirm that the C_6H_6 was benzene.

The unimolecular dissociation pathways of furan have been studied by ab initio electronic structure methods. Figure 13 is a composite summary of the potential energy surface for the decomposition of furan at 0 K. This figure is adapted from Sendt et al.[58] and results from G2(MP2) calculations. The energies for C−H rupture (shown in blue) or C−C cleavage (shown in red) are predicted to be 122 and 89 kcal mol^{-1}. Both C−H bond energies to produce the α-C_4H_3O and β-C_4H_3O furyl radicals (of $^2A'$ symmetry) are much larger than the C−H bond energy of benzene itself.[59] Consequently, it is predicted that all of the fragmentation processes of furan ensue following rearrangement to either the α-carbene (which directly fragments to HCCH + $CH_2{=}C{=}O$) or the β-carbene. The β-carbene isomerizes to buta-2,3-dienal, $CH_2{=}C{=}CH{-}CHO$, which decomposes to CO + CH_3CCH.

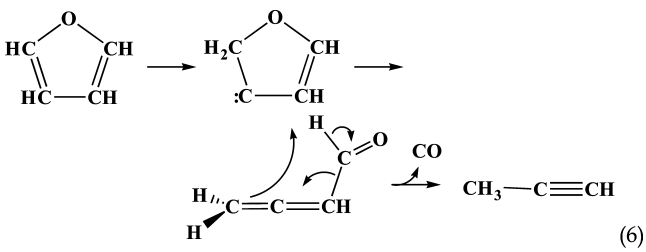

(6)

The propargyl radical (CH_2CCH, $^2B_1$) could result from the intermediate aldehyde in eq 6. It is predicted[58] that the C−C bond energy of buta-2,3-dienal is about 3 eV, ΔH_{298}($CH_2{=}C{=}CH{-}CHO \rightarrow CH_2CCH + CHO$) = 74 kcal mol^{-1}. Following the 65 μs thermal cracking of furan in the tubular reactors in Figures 3 and 4, we observe all but one of the direct products predicted[58] by the G2(MP2) calculations, HCCH + CH_2CO + CH_3CCH + CO + CH_2CCH + HCO. With the exception of the formyl radical, all other species have been identified by mass spectroscopy and infrared spectroscopy. One would not expect[34] the formyl radical to survive for very long in the hot tubular reactor. The ΔH_{298}(H−CO) is only 15.6 ± 0.1 kcal mol^{-1}; therefore, HCO is easily dissociated. Consequently, it is expected that $CH_2{=}C{=}CH{-}CHO \rightarrow CH_3C{\equiv}CH$ + CO + H.

The experimental results of this paper demonstrate that the first thermal dissociation products of furan (**1** in Figure 2) are (CO + CH_3CCH) and (HCCH + $CH_2{=}C{=}O$). At higher temperatures, furan also cracks to generate the propargyl radical. At low pressures in the tubular reactor, these molecules are all prompt products from furan and are formed in less than 100 μs (see Figure 1). At higher pressures in the tubular reactor, radicals such as CH_2CCH react further to produce complex aromatic gasification products such as C_6H_6 (benzene) and $C_6H_5CH{=}CH_2$ (styrene).

Acknowledgment. This research was supported by the DOE's National Renewal Energy Laboratory (Contract No. 1544759) and by grants from the Chemical Physics Program, United States Department of Energy (DE-FG02-93ER14364) and the National Science Foundation (CHE-0848606). We are grateful to Dr. Hans-Heinrich Carstensen, Dr. David Robichaud, and Dr. Krzysztof M. Piech for stimulating discussions.

References and Notes

(1) *A Survey of Biomass Gasification*; Reed, T. B., Ed.; Solar Energy Research Institute: Golden, CO, 1979; Vol. II, Principles of Gasification.
(2) Bridgewater, A. V. *Fuel* **1995**, *74*, 631.
(3) Yaman, S. *Energy Convers. Manage.* **2004**, *45*, 651.
(4) Shafizadeh, F. *J. Anal. Appl. Pyrolysis* **1982**, *3*, 283.
(5) Antal, M. J.; Varhegyi, G.; Jakab, E. *Ind. Eng. Chem. Res.* **1998**, *37*, 1267.
(6) Diebold, J. P. *Biomass Bioenergy* **1994**, *7*, 75.
(7) Antal, M. J.; Varhegyi, G. *Ind. Eng. Chem. Res.* **1995**, *34*, 703.
(8) Nishiyama, Y.; Langan, P.; Chanzy, H. *J. Am. Chem. Soc.* **2002**, *124*, 9074.
(9) O'Sullivan, A. C. *Cellulose* **1997**, *4*, 173.
(10) Matthews, J. F.; Skopec, C. E.; Mason, P. E.; Zuccato, P.; Torget, R. W.; Sugiyama, J.; Himmel, M. E.; Brady, J. W. *Carbohydr. Res.* **2006**, *341*, 138.
(11) Beaumont, O. *Wood Fiber Sci.* **1985**, *17*, 228.
(12) Piskorz, J.; Radlein, D.; Scott, D. S. *J. Anal. Appl. Pyrolysis* **1986**, *9*, 121.
(13) Evans, R. J.; Milne, T. A. *Energy Fuels* **1987**, *1*, 123.
(14) Evans, R. J.; Milne, T. A. *Energy Fuels* **1987**, *1*, 311.
(15) Shafizadeh, F.; Lai, Y. Z. *J. Org. Chem.* **1972**, *37*, 278.
(16) Shafizadeh, F.; McGinnis, G. D.; Philpot, C. W. *Carbohydr. Res.* **1972**, *25*, 23.
(17) Shafizadeh, F.; Lai, Y. Z.; McIntyre, C. R. *J. Appl. Polym. Sci.* **1978**, *22*, 1183.
(18) Phillips, S. D. *Ind. Eng. Chem. Res.* **2007**, *46*, 8887.
(19) Grela, M. A.; Amorebieta, V. T.; Colussi, A. J. *J. Phys. Chem.* **1985**, *89*, 38.
(20) Hore, N. R.; Russell, D. K. *New J. Chem.* **2004**, *28*, 606.
(21) Fulle, D.; Dib, A.; Kiefer, J. H.; Zhang, Q.; Yao, J.; Kern, R. D. *J. Phys. Chem. A* **1998**, *102*, 7480.
(22) Organ, P. P.; Mackie, J. C. *J. Chem. Soc., Faraday Trans.* **1991**, *87*, 815.
(23) Bruinsma, O. S. L.; Tromp, P. J. J.; Nolting, H.; Moulijn, J. A. *Fuel* **1988**, *67*, 334.
(24) Lifshitz, A.; Bidani, M.; Bidani, S. *J. Phys. Chem.* **1986**, *90*, 5373.
(25) Friderichsen, A. V.; Shin, E. J.; Evans, R. J.; Nimlos, M. R.; Dayton, D. C.; Ellison, G. B. *Fuel* **2001**, *80*, 1747.
(26) Jochnowitz, E. B.; Zhang, X.; Nimlos, M. R.; Varner, M. E.; Stanton, J. F.; Ellison, G. B. *J. Phys. Chem. A* **2004**, *109*, 3812.
(27) Rohrs, H. W.; Wickham-Jones, C. T.; Berry, D.; Ellison, G. B.; Argrow, B. M. *Rev. Sci. Instrum.* **1995**, *66*, 2430.
(28) Zhang, X.; Friderichsen, A. V.; Nandi, S.; Ellison, G. B.; David, D. E.; McKinnon, J. T.; Lindeman, T. G.; Dayton, D. C.; Nimlos, M. R. *Rev. Sci. Instrum.* **2003**, *74*, 3077.

(29) Friderichsen, A. V.; Radziszewski, J. G.; Nimlos, M. R.; Winter, P. R.; Dayton, D. C.; David, D. E.; Ellison, G. B. *J. Am. Chem. Soc.* **2001**, *123*, 1977.

(30) Nandi, S.; Arnold, P. A.; Carpenter, B. K.; Nimlos, M. R.; Dayton, D. C.; Ellison, G. B. *J. Phys. Chem. A* **2001**, *105*, 7514.

(31) Nandi, S.; Blanksby, S. J.; Zhang, X.; Nimlos, M. R.; Dayton, D. C.; Ellison, G. B. *J. Phys. Chem. A* **2002**, *106*, 7547.

(32) Chen, P.; Colson, S. D.; Chupka, W. A.; Berson, J. A. *J. Phys. Chem.* **1986**, *90*, 2319.

(33) Brown, A. L.; Dayton, D. C.; Nimlos, M. R.; Daily, J. W. *Energy Fuels* **2001**, *15*, 1276.

(34) Blanksby, S. J.; Ellison, G. B. *Acc. Chem. Res.* **2003**, *36*, 255.

(35) Pedley, J. B.; Naylor, R. D.; Kirby, S. P. *Thermochemistry of Organic Compounds*, 2 ed.; Chapman and Hall: New York, 1986. The 298 K enthalpies of formation are CO (-26.42 ± 0.04 kcal mol^{-1}), CH_3CCH (44.2 ± 0.2 kcal mol^{-1}), HCCH (54.3 ± 0.2 kcal mol^{-1}), and CH_2CO (-11.4 ± 0.4 kcal mol^{-1}).

(36) Herzberg, G. H. *Molecular Spectra and Molecular Structure: Electronic Spectra and Electronic Structure of Polyatomic Molecules*; D. Van Nostrand: Princeton, NJ, 1967; Vol. III.

(37) Baker, C.; Turner, D. W. *Proc. R. Soc. London* **1968**, *308*, 19; $IE(CH_3CCH) = 10.37 \pm 0.01$ eV.

(38) Hall, D.; Maier, J. P.; Rosmus, P. *Chem. Phys.* **1977**, *24*, 373.

(39) Niu, B. H.; Bai, Y.; Shirley, D. A. *J. Chem. Phys.* **1993**, *99*, 2520; $IE(CH_2CO) = 9.6191 \pm 0.0004$ eV.

(40) Gilbert, T.; Pfab, R.; Fischer, I.; Chen, P. *J. Chem. Phys.* **2000**, *112*, 2575.

(41) Lau, K. C.; Ng, C. Y. *Acc. Chem. Res.* **2006**, *39*, 823.

(42) Erman, P.; Karawajczyk, A.; Rachlewkallne, E.; Stromholm, C.; Larsson, J.; Persson, A.; Zerne, R. *Chem. Phys. Lett.* **1993**, *215*, 173.

(43) Chewter, L. A.; Sander, M.; Müller-Dethlefs, K.; Schlag, E. W. *J. Chem. Phys.* **1987**, *86*, 4737; $IE(C_6H_6) = 9.24372 \pm 0.00005$ eV.

(44) Lipert, R. J.; Colson, S. D. *J. Phys. Chem.* **1990**, *94*, 2358; $IE(C_6H_5OH) = 8.508 \pm 0.001$ eV.

(45) Dyke, J. M.; Ozeki, H.; Takahashi, M.; Cockett, M. C. R.; Kimura, K. *J. Chem. Phys.* **1992**, *97*, 8926; $IE(C_6H_5CH{=}CH_2) = 8.464 \pm 0.001$ eV.

(46) Robinson, M. S.; Polak, M. L.; Bierbaum, V. M.; DePuy, C. H.; Lineberger, W. C. *J. Am. Chem. Soc.* **1995**, *117*, 6766; $DH_{298}(H{-}CH_2CCH) = 90 \pm 3$ kcal mol^{-1}; enthalpy of formation (298 K) (CH_2CCH) $= 82.5 \pm 3.0$ kcal mol^{-1}.

(47) Alkemade, U.; Homann, K. H. *Z. Phys. Chem.* **1989**, *161*, 19.

(48) Morter, C. L.; Farhat, S. K.; Adamson, J. D.; Glass, G. P.; Curl, R. F. *J. Phys. Chem.* **1994**, *98*, 7029.

(49) Atkinson, D. B.; Hudgens, J. W. *J. Phys. Chem. A* **1999**, *103*, 4242.

(50) Fahr, A.; Nayak, A. *Int. J. Chem. Kinet.* **2000**, *32*, 118.

(51) Scherer, S.; Just, T.; Frank, P. *Proc. Combust. Inst.* **2000**, *28*, 1511.

(52) Miller, J. A.; Klippenstein, S. J. *J. Phys. Chem. A* **2001**, *105*, 7254.

(53) DeSain, J. D.; Taatjes, C. A. *J. Phys. Chem. A* **2003**, *107*, 4843.

(54) Miller, J. A.; Klippenstein, S. J. *J. Phys. Chem. A* **2003**, *107*, 7783.

(55) Shafir, E. V.; Slagle, I. R.; Knyazev, V. A. *J. Phys. Chem. A* **2003**, *107*, 8893.

(56) Tang, W. Y.; Tranter, R. S.; Brezinsky, K. *J. Phys. Chem. A* **2005**, *109*, 6056.

(57) Tang, W. Y.; Tranter, R. S.; Brezinsky, K. *J. Phys. Chem. A* **2006**, *110*, 2165.

(58) Sendt, K.; Bacskay, G. B.; Mackie, J. C. *J. Phys. Chem. A* **2000**, *104*, 1861.

(59) Ervin, K. M.; DeTuri, V. F. *J. Phys. Chem. A* **2002**, *106*, 9947; $D_0(C_6H_5{-}H) = 111.3 \pm 0.5$ kcal mol^{-1} and $DH_{298}(C_6H_5{-}H) = 112.9 \pm 0.5$ kcal mol^{-1}.

JP903401H